HHS Public Access

Author manuscript

ACS Appl Mater Interfaces. Author manuscript; available in PMC 2024 August 30.

Published in final edited form as:

ACS Appl Mater Interfaces. 2024 March 06; 16(9): 11159–11171. doi:10.1021/acsami.3c14908.

Cell-Penetrating and Enzyme-Responsive Peptides for Targeted Cancer Therapy: Role of Arginine Residue Length on Cell Penetration and In Vivo Systemic Toxicity

Behnaz Ghaemi[○],
Russell H. Morgan Department of Radiology and Radiological Science, Division of MR Research and Cellular Imaging Section and Vascular Biology Program, Institute for Cell Engineering, The Johns Hopkins University School of Medicine, Baltimore, Maryland 21205, United States

Swati Tanwar[○],
Department of Mechanical Engineering, The Johns Hopkins University Whiting School of Engineering, Baltimore, Maryland 21218, United States

Aruna Singh,
F.M. Kirby Research Center for Functional Brain Imaging, Kennedy Krieger Inc., Baltimore, Maryland 21205, United States

Dian R. Arifin,
Russell H. Morgan Department of Radiology and Radiological Science, Division of MR Research and Cellular Imaging Section and Vascular Biology Program, Institute for Cell Engineering, The Johns Hopkins University School of Medicine, Baltimore, Maryland 21205, United States

Michael T. McMahon,
Russell H. Morgan Department of Radiology and Radiological Science, Division of MR Research, The Johns Hopkins University School of Medicine, Baltimore, Maryland 21205, United States; F.M. Kirby Research Center for Functional Brain Imaging, Kennedy Krieger Inc., Baltimore, Maryland 21205, United States

Ishan Barman,

Corresponding Authors: Ishan Barman – *Russell H. Morgan Department of Radiology and Radiological Science, Division of MR Research and Department of Oncology, The Johns Hopkins University School of Medicine, Baltimore, Maryland 21205, United States; Department of Mechanical Engineering, The Johns Hopkins University Whiting School of Engineering, Baltimore, Maryland 21218, United States;* ibarman@jhu.edu, **Jeff W. M. Bulte –** *Russell H. Morgan Department of Radiology and Radiological Science, Division of MR Research, Cellular Imaging Section and Vascular Biology Program, Institute for Cell Engineering, Department of Biomedical Engineering, and Department of Oncology, The Johns Hopkins University School of Medicine, Baltimore, Maryland 21205, United States; F.M. Kirby Research Center for Functional Brain Imaging, Kennedy Krieger Inc., Baltimore, Maryland 21205, United States; Department of Chemical and Biomolecular Engineering, The Johns Hopkins University Whiting School of Engineering, Baltimore, Maryland 21218, United States;* jwmbulte@mri.jhu.edu.

[○]Author Contributions

B.G. and S.T. contributed equally to this work.

The authors declare no competing financial interest.

ASSOCIATED CONTENT

Supporting Information

The Supporting Information is available free of charge at https://pubs.acs.org/doi/10.1021/acsami.3c14908.

Toxicity of R_1–R_6AANCK peptides toward LNCaP and kidney and liver histology images (PDF)

Complete contact information is available at: https://pubs.acs.org/10.1021/acsami.3c14908

Russell H. Morgan Department of Radiology and Radiological Science, Division of MR Research and Department of Oncology, The Johns Hopkins University School of Medicine, Baltimore, Maryland 21205, United States; Department of Mechanical Engineering, The Johns Hopkins University Whiting School of Engineering, Baltimore, Maryland 21218, United States

Jeff W. M. Bulte
Russell H. Morgan Department of Radiology and Radiological Science, Division of MR Research, Cellular Imaging Section and Vascular Biology Program, Institute for Cell Engineering, Department of Biomedical Engineering, and Department of Oncology, The Johns Hopkins University School of Medicine, Baltimore, Maryland 21205, United States; F.M. Kirby Research Center for Functional Brain Imaging, Kennedy Krieger Inc., Baltimore, Maryland 21205, United States; Department of Chemical and Biomolecular Engineering, The Johns Hopkins University Whiting School of Engineering, Baltimore, Maryland 21218, United States

Abstract

For the improved delivery of cancer therapeutics and imaging agents, the conjugation of cell-penetrating peptides (CPPs) increases the cellular uptake and water solubility of agents. Among the various CPPs, arginine-rich peptides have been the most widely used. Combining CPPs with enzyme-responsive peptides presents an innovative strategy to target specific intracellular enzymes in cancer cells and when combined with the appropriate click chemistry can enhance theranostic drug delivery through the formation of intracellular self-assembled nanostructures. However, one drawback of CPPs is their high positive charge which can cause nonspecific binding, leading to off-target accumulation and potential toxicity. Hence, balancing cell-specific penetration, toxicity, and biocompatibility is essential for future clinical efficacy. We synthesized six cancer-specific, legumain-responsive R_nAANCK peptides containing one to six arginine residues, with legumain being an asparaginyl endopeptidase that is overexpressed in aggressive prostate tumors. When conjugated to Alexa Fluor 488, R_1–R_6AANCK peptides exhibited a concentration- and time-dependent cell penetration in prostate cancer cells, which was higher for peptides with higher R values, reaching a plateau after approximately 120 min. Highly aggressive DU145 prostate tumor cells, but not less aggressive LNCaP cells, self-assembled nanoparticles in the cytosol after the cleavage of the legumain-specific peptide. The *in vivo* biocompatibility was assessed in mice after the intravenous injection of R_1–R_6AANCK peptides, with concentrations ranging from 0.0125 to 0.4 mmol/kg. The higher arginine content in $R_{4–6}$ peptides showed blood and urine indicators for the impairment of bone marrow, liver, and kidney function in a dose-dependent manner, with instant hemolysis and morbidity in extreme cases. These findings underscore the importance of designing peptides with the optimal arginine residue length for a proper balance of cell-specific penetration, toxicity, and *in vivo* biocompatibility.

Graphical Abstract

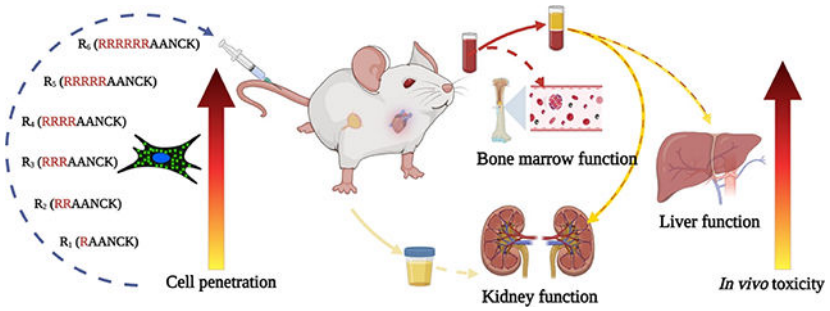

Keywords

enzyme-responsive peptide; cell-penetrating peptide; legumain; arginine; biocompatibility

1. INTRODUCTION

Cancer cells have evolved biological mechanisms to restrict the uptake of xenobiotics.[1] Consequently, the physical properties of many therapeutics prevent penetration through the polar extracellular microenvironment and diffusion into the nonpolar cancer cell membrane. This opposing polarity can be overcome by conjugating bipolar transporter molecules that improve water solubility and cellular uptake.[2] Cell-penetrating peptides (CPPs) represent promising bipolar transporters for therapeutic drug delivery with significant pharmaceutical applications.[3] The interaction between cells and peptides depends on various factors, including the amino acid composition, molecular weight, sequence length, total electric charge, hydrophobicity, isoelectric point, amphiphilicity, and ultimate configuration.[4] Studies have shown that the affinity of peptide transporters for biomembranes is rooted in their arginine-rich subsequences.[5] Arginine-rich peptides such as TAT (YGRKKRRQRRR) and CTP (YGRRARRRRRR) are able to carry various types of cancer therapeutics by penetrating through cell membranes *in vitro* and *in vivo*.[6,7] Their multiple conjugation sites and ability to induce apoptosis make them promising candidates for enhancing the effectiveness of chemotherapy and reducing off-target accumulation and side effects.[8] Recent studies have revealed that hybrid peptide systems containing a combination of mitochondria-targeted and cell-penetrating peptides possess the capability to induce apoptosis in cancer cells by disrupting the mitochondria and activating pro-apoptotic pathways.[9] This mechanism has the potential to inhibit tumor growth and increase the tumor's susceptibility to chemotherapy. Arginine-rich CPPs can also activate immune cells and enhance their antitumor activity, potentially improving tumor control and leading to long-term remission.[10]

CPPs are now being combined with enzyme-responsive peptide sequences to develop tumor-specific therapeutic and diagnostic platforms.[11] Enzyme-specific recognition motifs have gained much attention due to the enzyme's ability to cleave specific peptide bonds with precise spatiotemporal control. This catalytic prowess has inspired the creation of novel classes of synthetic peptide-based theranostic nanoprobes for enhanced imaging and tumor-targeted therapy.[12] In the recent past, we have explored enzyme-responsive peptide sequences to advance targeted tumor imaging/therapy using chemical exchange

saturation transfer magnetic resonance imaging (CEST MRI),[13] Raman imaging,[14,15] and quantitative phase imaging (QPI).[16] While enzyme responsiveness enables successful nanoprobe accumulation in most living systems *in vitro*, the efficacy of *in vivo* intracellular applications is heavily dependent on the local probe concentration, as dictated by the unpredictable *in vivo* tumor macro- and microenvironments. Consequently, strategies to maximize tumor cell penetration are imperative.

However, the initial transport of the CPP+enzyme-responsive peptide across the cell membrane is not cancer cell-specific and may lead to unwanted toxicity to normal cells at higher peptide concentrations.[17,18] The high positive charge of these peptides can cause nonspecific binding and destabilization of the negatively charged cell membrane, potentially resulting in cell lysis and death.[19] The toxicity of arginine-rich peptides may be modulated by a number of factors, including the peptide concentration, peptide length, and presence of specific amino acid residues. While arginine-rich peptides have demonstrated their potential in cancer therapy, a careful evaluation of their *in vivo* biocompatibility as a function of peptide length is warranted in order to mitigate their potential toxic side effects. To this end, we designed a series of novel prostate cancer-specific legumain enzyme-responsive peptides, $R_{1–6}$AANCK, containing one to six (R_1–R_6) arginine residues. In addition to the enzyme responsiveness to the RAANCK sequence, we report here on the time- and concentration-dependent cell penetration *in vitro*, as well as the biocompatibility and toxicity *in vivo*.

2. MATERIALS AND METHODS

2.1. Cell Penetration and Intracellular Legumain-Mediated Nanoparticle Formation.

2.1.1. Synthesis and Characterization of Alexa Fluor 488-Conjugated R_1–R_6 AANCK Peptides.—

R_1–R_6 AANCK peptides were purchased from Genscript and were used for Alexa Fluor 488 (Invitrogen, USA) conjugation without further purification. Ten milligrams of R_1–R_6 AANCK peptides was first dissolved in 1 mL of dry N,N-dimethylformamide (DMF, Chemimpex, USA), followed by the addition of 10 mL of diisopropylethylamine (DIPEA, Chemimpex, USA), and then Alexa Fluor 488 NHS ester (1 mg in 200 mL of dry DMF). The mixture was stirred at room temperature in the dark for 2 h. Alexa Fluor 488-conjugated peptides were purified by reverse-phase high-performance liquid chromatography (RP-HPLC) using a Shimadzu CBM-40 system with a C18 column. A water–acetonitrile eluent (from 80:20 to 20:80) containing 0.1% TFA was used as the mobile phase for purification. The mass of the synthesized peptides (Figure 1) was determined using either Bruker Auto Flex III or Voyager DE-STR high-resolution matrix-assisted laser desorption/ionization–time-of-flight (MALDI-TOF) mass spectrometers. The yield of the Alexa Fluor 488-conjugated peptides was ~50%.

2.1.2. Determination of CP50 for Alexa Fluor 488-Conjugated R_1–R_6-AANCK Peptides.—

DU145 cells (American Type Culture Collection) were seeded in a 96-well plate and incubated for 24 h at 37 °C. A stock solution of the R_1–R_6-AANCK-Alexa Fluor 488 conjugate was prepared at 100 μM, followed by serial dilutions down to 0.1 μM. Post 24 h seeding, the cell medium was replaced with a peptide solution. After 60 and 120 min of incubation, cells were washed with 10 mM phosphate-buffered saline, pH 7.4

(PBS), to eliminate extracellular fluorescence. Fluorescence intensities were recorded using a plate reader, with the background fluorescence subtracted. The peptide concentration at which cells reached 50% of the maximum fluorescence (CP50) was then calculated.[20] Cells incubated with Alexa Fluor 488 alone and untreated cells were used as controls.

2.1.3. Qualitative Time-Dependent Cell Penetration Studies.—DU145 cells were cultured in 24-well plates containing a 15 mm coverslip at the bottom. Once the cells reached 70% confluency, the culture medium was replaced with MEM Glutamax medium (Gibco, USA) containing 50 μ*M* Alexa Fluor 488-R_1–R_6AANCK peptides. Following 120 min incubation, cells were washed with PBS (Gibco, USA) and then fixed with 4% paraformaldehyde (PFA) for 20 min. Nuclei were counterstained with 4′,6-diamidino-2-phenylindole (DAPI), and the coverslips were mounted on glass slides. Cells were analyzed using an inverted epifluorescence microscope (Zeiss Axiovert 200M).

2.1.4. Quantitative Time-Dependent Cell Penetration Studies.—DU145 prostate cancer cells were cultured in 96-well plates for 24 h to achieve 70% confluency. Cells were incubated with 50 μ*M* of Alexa Fluor 488-R_1–R_6 peptides in MEM Glutamax media for 30, 60, 90, 120, or 180 min in the dark. After washing three times with 10 mM PBS, pH 7.4 (PBS), the fluorescence intensity was measured using a plate reader (Thermo Scientific, USA) at an excitation wavelength of 488 nm.

2.1.5. Synthesis and Characterization of Legumain Responsive Peptide Sequences and Nanoparticle Formation.

2.1.5.1. Synthesis of R_6 AANCK Peptide.: The peptide R_6AANCK was synthesized using a solid-phase peptide synthesis (SPPS) method with 2-chlorotrityl chloride (CTC) resins using an AAPPTEC focus Xi peptide synthesizer. The N-terminus of the peptide was acetylated by treatment with 5% acetic anhydride in dimethylformamide (DMF) for 10 min. After sequential washing with DMF and dichloromethane (DCM), resins were treated with 2% TFA/DCM to cleave the peptide from the resin without removing the 2,2,4,6,7-pentamethyldihydrobenzofuran-5-sulfonyl residue (Pbf), *tert*-butyloxycarbonyl (BOC), and S-*tert*-butylthio (StBu) protecting groups of arginine, lysine, and cysteine, respectively. The protected R_6 AANCK peptide was produced after evaporating the solvent using a rotary evaporator, followed by recrystallization with ice-cold diethyl ether.

2.1.5.2. CBT Conjugation of R_6 AANCK Peptide.: The protected peptide (300 mg) was dissolved in 15 mL of anhydrous tetrahydrofuran (THF), followed by the addition of 33 μL of 4-methylmorpholine (MMP). The reaction mixture was stirred for 30 min at 0 °C under a N_2 gas atmosphere, followed by the addition of 38.9 μL of isobutyl chloroformate (IBCF) with additional stirring for 40 min. A solution of 31.5 mg of CBT in 1 mL of THF and 6.4 μL of IBCF was added to the reaction mixture with continued stirring for 1 h at 0 °C and then stirred overnight at RT. The CBT-conjugated R_6 AANCK peptide was precipitated from the reaction mixture using diethyl ether and dried. The Boc- and Pbf-protecting groups of compound B were cleaved with a cleavage cocktail having 95% TFA, 4% DCM, and 1.0% triisopropylsilane (TIPS) for 4 h. The R_6 AANCK-CBT peptide was purified by RP-HPLC

using water–acetonitrile, with 0.1% TFA as the eluent (from 80:20 to 20:80). The yield of CBT conjugation was found to be 30%.

2.1.5.3. Alexa Fluor 488 Conjugation of R_6 AANCK-CBT Peptide.: Alexa Fluor 488 NHS ester (1 mg) was dissolved in 500 μL of anhydrous DMF and 10 μL of DIPEA. A solution of 10 mg R_6 AANCK-CBT peptide in DMF was added, and the reaction mixture was stirred for 2 h in the dark at RT. The Alexa Fluor 488-conjugated peptide was obtained following purification using RP-HPLC with a 50% yield.

2.1.5.4. Legumain Expression.: Legumain expression in DU145 and LNCaP cells was determined using immunostaining and an inverted epifluorescence microscope (Zeiss Axiovert 200M), with the quantification of fluorescence intensity using ZEN software. DU145 and LNCaP cells were cultivated on chamber slides until they reached approximately 70% confluency. After washing with PBS, cells were fixed with 4% PFA for 10 min. The fixed cells were then incubated with antilegumain antibody (1:500, ab183028, Abcam, USA) overnight at 4 °C. Cells were washed three times with PBS and then treated with secondary antibody goat antirabbit IgG-Alexa Fluor 488 (1:250, ab150077, Abcam, USA) and Alexa Fluor 594 phalloidin to visualize cell borders. After further washing, they were stained with DAPI, coverslipped, and imaged using a Zeiss Axiovert 200 M inverted epifluorescence microscope.

2.1.5.5. Intracellular Self-Assembly of Nanoparticles.: To examine the intracellular self-assembly of the nanoparticles, DU145 and LNCaP cells were cultured on chamber slides until they reached approximately 70% confluency. They were treated with a 3 μM solution of Alexa Fluor 488-conjugated R6 AANCK-CBT for 3 h at 37 °C, followed by replacement with fresh media and additional incubation for 30 min. Cells were washed with PBS three times and fixed with 4% PFA for 20 min, resuspended back in PBS, and then imaged using a Leica SP8 confocal microscope equipped with a 63x oil immersion objective.

2.2. *In Vitro* Cytotoxicity Assay.

DU145 and LNCaP cells were cultured in 96-well plates to 70% confluency and incubated with different concentrations (3.125, 6.25, 12.5, 25, 50, and 100 mM) of the R_1–R_6AANCK peptides for 2 or 48 h. The culture medium was collected and centrifuged at 10,000 × *g* for 10 min to eliminate cellular debris. The lactate dehydrogenase (LDH) activity was quantified in the collected medium using an LDH assay kit (Abcam, USA) as per the manufacturer's instructions.

2.3. Hemolytic Assay.

Blood samples were withdrawn using a 1 mL syringe with a 26G needle from the heart of female $Rag2^{-/-}$ mice, collected in a 1 mL BD Microtainer (Becton Dickinson, USA) containing EDTA as an anticoagulant, and stored at 4 °C before further analysis. One milliliter of whole blood sample was centrifuged at 1500 × *g* for 5 min, the resulting plasma fraction was removed, and the pellets were washed with 1 mL of PBS after mixing by slow inversion. Centrifugation and washing steps were repeated five times. After the final washing step, PBS was added, and the resulting samples were diluted 1:10 with PBS to yield

a red blood cell (RBC) concentration of approximately 5×10^8 RBCs/mL. The hemolytic assay was performed in a 96-well polypropylene microplate containing 50 μL of RBCs by adding R_1–R_6 peptides at different concentrations (3.125, 6.25, 12.5, 25, 50, and 100 mM) in 50 μL of PBS. 1% Triton-X100 (50 μL) in water or PBS was added to the RBCs as positive and negative (diluent) controls, respectively. The plate was sealed, shaken on a plate shaker for 20 s, and incubated for 1 h in a 37 °C incubator. The microplate was centrifuged at 1500*g* for 5 min, and 80 μL of supernatant was removed from each well and transferred to a new 96-well microplate. After the air bubbles were removed by centrifugation of the microplate at 1200*g* for 1 min, the optical density was measured at 405 nm using a plate reader (Thermo Scientific, USA). The percentage of hemolysis was calculated using the following equation:

$$\% \text{ Hemolysis} = \frac{(\text{absorbance of test sample}) - (\text{absorbance of negative control})}{(\text{absorbance of positive control}) - \text{absorbance of negative control}} \times 100$$

2.4. *In Vivo* Toxicity Assays.

All animal experiments were approved by the Institutional Animal Care and Use Committee. Immunodeficient $Rag2^{-/-}$ breeder mice were purchased from Jackson Laboratory (Bar Harbor, ME, USA), and an in-house colony was maintained under a 12 h light/dark cycle with free access to food and water. All experiments were performed using 1% isoflurane inhalation anesthesia. Female $Rag2^{-/-}$ mice (20–25 g, $n = 3$ for each cohort, $n = 18$ total)) were injected intravenously (i.v., tail vein) with 0.0125, 0.025, 0.05, 0.1, 0.2, or 0.4 mmol/kg R_1–R_6AANCK peptide in 100 μL of PBS containing 5% dimethyl sulfoxide (DMSO). One week after injection, blood was collected from the heart using a 1 mL syringe with a 26G needle and urine from the bladder using a 0.5 mL syringe with a 28G needle.

2.5. Assessment of Bone Marrow Function.

For total cell blood counts (CBC), 100 μL of fresh blood was transferred into a 100 μL microvette tube (Sarstedt AG&Co, Germany) containing EDTA as an anticoagulant, mixed gently, and stored at 4 °C until further CBC analysis.

2.6. Assessment of Liver Function.

For liver function tests, 450 μL of fresh blood was transferred into a 1 mL BD Microtainer (Becton, Dickinson and Company, NJ, USA) and allowed to sit for 30 min at room temperature before centrifugation for 10 min at 1500*g*. The plasma supernatant was collected and sent to IDEXX (Main, USA) for biochemical analysis.

2.7. Assessment of Kidney Function.

Creatinine, uric acid, blood urea nitrogen, albumin, and total protein levels in blood plasma were measured to evaluate the kidney function. The presence of creatinine and total protein as waste products in urine was also assessed. The plasma and urine samples were sent to IDEXX (Maine, USA) for biochemical analysis.

2.8. Histopathology of Liver and Kidney.

Liver and kidney were harvested for H&E staining 7 days after i.v. injection of R_{1-6}AANCK. Tissue sections (10 μm thick) were obtained using a microtome, deparaffinized in xylene, and rehydrated through a descending alcohol gradient. After staining, the sections were dehydrated, cleared, and mounted on a coverslip using a xylene-based mounting medium. The sections were imaged by using a Zeiss Axiovert 200 M inverted epifluorescence microscope.

2.9. Statistical Analysis.

Statistical analysis was performed using one-way ANOVA with Tukey's HSD multiple comparison posthoc test. Data are shown as mean ± SD (n = 3 independent experiments). P-values <0.0001 (****), < 0.001 (***), < 0.01 (**), and <0.05 (*) were considered significant.

3. RESULTS AND DISCUSSION

3.1. R_1–R_6-AANCK Peptide Synthesis, Characterization, and Concentration-Dependent Cellular Uptake.

To improve the targeting efficacy of anticancer agents, there has been a shift toward designing stimuli-responsive therapeutic carriers.[21] These carriers respond to specific cues in the tumor microenvironment, allowing for enhanced accumulation of anticancer agents while minimizing off-target effects. One of the more promising smart strategies involves the use of enzyme-responsive peptide sequences.[11] This approach has gained momentum due to the growing evidence linking cancer cell invasion, metastasis, and angiogenesis to dysregulated enzyme expression.[22] To align our study with the relevant biological studies, we designed polyarginine peptide sequences with a legumain enzyme recognition motif: alanine–alanine–asparagine (AAN) bound to CK (AANCK), where cysteine facilitates self-assembly into nanostructures and lysine facilitates linkage to imaging probes such as Alexa Fluor 488 (optical probe) or olsalazine (CEST MRI probe).[13] Since legumain is an asparaginyl endopeptidase that is overexpressed in tumor cells exhibiting aggressive migration and invasion,[23–26] it is an attractive candidate as a tumor-associated enzyme for enhanced therapy and imaging.[27,28] The exact sequence and chemical structure of all peptides used in this study are shown in Table 1. Successful synthesis of R_1–R_6 peptides and their Alexa Fluor 488-conjugated counterparts (for the visualization of intracellular internalization) was verified using MALDI-TOF spectrometry (Figure 1).

We measured the concentration-dependent uptake of the synthesized peptides in DU145 cells and found that the intensity of Alexa Fluor 488 correlates directly with the cytosolic levels of R_1–R_6-AANCK. This was verified by recording the fluorescence intensity corresponding to the half-maximum cell penetration concentration (CP50) over varying incubation periods with DU145 cells (Table 1). After 60 min of incubation, R_6 exhibited the lowest CP50 at 0.8 μM (corresponding to the highest cellular uptake). The CP50 values for R_5, R_4, R_3, R_2, and R_1 followed with concentrations of 1.3, 3.2, 8.5, 30, and 75 μM, respectively. However, when the incubation time was extended to 120 min, the temporal dynamics changed. For R_6, R_5, and R_4, an increase in CP50 to 2.1, 5.2, and 7.8 μM was

noted, respectively, suggesting a decrease in cellular uptake or a potential washout of the peptide post 60 min. In contrast, CP50 of R3 remained relatively constant at 8.9 μM over the extended period, while for R_2 and R1, the longer incubation led to increased cellular uptake with decreased CP50 values of 12 and 32 μM, respectively. The peptides with lower arginine content (R_1 and R_2) thus showed a trend toward increased uptake with longer incubation, whereas peptides with higher arginine content (R_6, R_5, and R_4) had the opposite trend. This could potentially be attributed to varying peptide stability, surface charge, or internalization mechanisms, warranting further exploration. Other studies on arginine-rich CPPs including TAT (RKKRRQRRR), penetratin (RQI - KIWFQNRRMKWKK), and nona-arginine (9R), when tagged with chloroalkane, reported a concentration-dependent cytosolic localization after 4 h, with CP50 values of 3.1, 0.82, and 0.3 μM, respectively.[29]

3.2. Time-Dependent Cell Penetration Studies.

We examined the time-dependent cell penetration of R_1–R_6AANCK peptides, each with varying lengths of arginine residues, at a concentration of 50 μM to encompass the CP50 values for all peptides. Peptides were conjugated with Alexa Fluor 488 to allow the quantitative fluorescence detection of cell penetration at 30, 60, 90, 120, and 180 min after addition to DU145 prostate cancer cells (Figure 2A,B). Overall, the rate of peptide penetration decreased with a decrease in the number of arginine residues, in agreement with a previous report demonstrating the importance of the arginine residue length for cellular internalization of CPPs.[30] For the higher arginine residue peptides (R_5 and R_6), the highest penetration rate (fluorescence intensity) was observed at 30 min, followed by a steep decline, while all other peptides ($R_{1–4}$) showed an initial gradual increase that reached a maximum around 120 min. At 180 min, all of the peptides were nearly washed out. The cell penetration at 60 min after the peptide addition was further evaluated by a qualitative assessment using fluorescence microscopy (Figure 2C). The resulting uptake and internalization were consistent with the quantitative fluorescence intensity measurements.

Previous studies have shown that increasing the number of arginine residues in linear peptides from 6 to 9 can lead to a heightened cell penetration in HeLa cancer cells after 30 min of incubation with 5 μM peptide.[31] In addition, it was reported that the inclusion of four endocyclic and three exocyclic arginine residues within macrocyclic peptides is more effective in increasing cell penetration than incorporating six arginines in bicyclic peptides.[32] Our study clearly demonstrates that arginine-rich peptides containing four, five, and six arginine residues exhibit significantly greater attachment to negatively charged molecules on the cell surface within a 30–60 min time frame compared to peptides containing one, two, and three arginine residues. This suggests that the presence of a higher number of arginine residues plays a crucial role in facilitating cellular uptake of the peptides, rather than the overall positive peptide charge.[33] However, other studies on conjugating of R_4, R_8, R_{12}, and R_{16} peptides to extracellular vesicles (EVs) for enhancing uptake in HeLa cells indicated that R_8 was the most effective promotor after 30 min of incubation.[34]

Arginine-rich CPPs can penetrate cell membranes spontaneously and without the need for energy by directly interacting with acidic lipids in the outer leaflet of the membrane.[35] Studies have shown that arginine-rich peptides undergo a two-step uptake process, beginning

with the initial attachment to the cell membrane.[36] This attachment is influenced mainly by electrostatic interactions between the negatively charged molecules on the cell surface and positively charged arginine.[37] Since the fraction of acidic-charged phospholipids in biological plasma membranes is low, it is believed that positively charged arginine-rich peptides bind to negatively charged sulfated glycosaminoglycans (GAGs) to facilitate cell membrane penetration.[38] The interaction of arginine-rich peptides with sulfated GAGs may play a critical role in their direct membrane translocation, which involves the peptides crossing the membrane rather than being taken up by endocytosis.[39] These interactions may lead to a charge neutralization of arginine-rich CPPs, promoting their partitioning into cell membranes.[40,41] The second uptake step involves translocation across the cell membrane, which depends on peptide neutrality and size.[42,43] Recent research also suggests that the most plausible mechanism for the direct membrane translocation of arginine-rich peptides is the transient formation of pores, where the peptides induce membrane perturbation to facilitate their passage through the membrane.[44] Smaller and less positively charged peptides have a greater capacity to traverse the lipophilic membrane and reach the cytoplasm more rapidly.[45] Other ways of modulating the transport of arginine-rich peptides include increasing the distance between arginine residues for the promotion of cellular uptake.[18] A greater spacing allows for more flexibility in receptor binding for turnover or to associate with negatively charged species on the surface of cells, which is necessary for internalization. Through the comparative analysis of R_4, R_5, and R_6 peptides, they showed that an increase in the arginine content corresponds to an acceleration in cellular uptake rates.[46] In summary, depending on their composition, peptides may reach an equilibrium state in which cellular retention is balanced by uptake, efflux, and cellular degradation.

3.3. Legumain-Mediated Intracellular Self-Assembly of Fluorescent Nanoparticles.

Legumain is overexpressed in various tumors, in particular in prostate cancer,[47] being a lysosomal cysteine protease with an important function in cellular protein processing and maturation. This overexpression can be exploited for specific targeting, e.g., microbubble ultrasound contrast agents in breast cancer.[48] When we compared legumain expression in prostate cancer cell lines, a significant difference was observed between DU145 and LNCaP cells, both qualitatively (Figure 3A) and quantitatively (Figure 3B). DU145 cells, known for their high tumor aggressiveness, exhibited markedly increased legumain levels compared to less aggressive LNCaP cells, implying a role for legumain in advanced protein processing that underpins tumor growth.[49] The acidity often associated with aggressive tumor environments may further amplify the legumain activity in DU145 cells.[50] Additionally, enhanced legumain expression can be instrumental in immune modulation, potentially providing DU145 cells with an advantage in immune evasion.[51] A modulation in signaling pathways, a characteristic of aggressive tumor cells, may also be associated with the heightened legumain activity.[52] To explore the responsiveness of legumain, the $R_{1–6}$AANCK peptides were conjugated to a CBT group and Alexa Fluor 488. After the legumain cleavage of the peptide, a biocompatible click condensation reaction between the glutathionine (GSH)-induced 1,2-aminothiol group (D-cysteine) and the cyano group of the (CBT) motif is initiated, resulting in the formation of clusters of aggregated Alexa Fluor 488 nanoparticles. This chemical reaction has been widely used for studying enzyme-responsive peptide sequences.[53–55] Upon the uptake of R_6AANCK-CBT-Alexa Fluor 488 peptides into

the cytoplasm of DU145 cells, these peptides undergo a controlled condensation reaction due to GSH reduction and legumain-induced peptide cleavage. This process results in the formation of dimer structures following a click reaction between two processed CBT-Alexa Fluor 488 molecules, driven by the legumain recognition of the AAN sequence. These dimers self-assemble into Alexa Fluor 488 nanoparticles as a result of intermolecular π–π stacking.[55] In LNCaP cells, the limited legumain expression restricts self-assembly, impeding the creation of alkyne-dimer nanoparticles.[56] Fluorescence microscopy shows extensive intracellular self-assembly of fluorescent NPs after the incubation of Alexa-R_6AAN-CBT peptide with DU145 cells but not LNCaP cells. Legumain is depicted in green, phalloidin in red, and the nucleus is stained blue (Figure 3C).

3.4. *In Vitro* Cytotoxicity Studies.

Assessment of cell membrane integrity is a widely employed technique to evaluate cell viability including the determination of the cytotoxic effects of arginine-rich peptides *in vitro*. To this end, we used an LDH cytotoxicity assay to assess both short- and long-term *in vitro* cytotoxicity in DU145 and LNCaP cells following incubation with R_1–R_6AANCK for 2 and 48 h, respectively. At 2 h, R_1-, R_2-, R_3-, and R_4-AANCK did not exhibit any toxicity at all concentrations tested (Figures 4A and S1A). R_5-AANCK only demonstrated 20% cytotoxicity at the highest concentration of 100 mM. In contrast, R_6-AANCK showed significant toxicity, with 15 and 30% cytotoxicity at concentrations of 50 and 100 mM, respectively. These findings clearly indicate that the observed increased initial cell penetration/membrane translocation of higher residue arginine peptides is associated with a concomitant loss of membrane integrity.

At 48 h, R_1-AANCK lacked cytotoxicity for all concentrations tested, while the other peptides demonstrated varying degrees of toxicity dependent on their concentration (Figures 4B and S1B). Compared to nonincubated control cells, the cytotoxicity of R_2–R_6AANCK peptides at the highest concentration (100 mM) ranged from 25 to 85%. Hence, cytotoxicity clearly depends on the overall arginine content and differs dramatically between 2 and 48 h incubation periods.

3.5. *InVivo* Toxicity Studies.

Intravenous administration of peptides with varying arginine lengths (R_1–R_6) and concentrations was performed to investigate their systemic *in vivo* toxicity in mice. The R_1AANCK peptide did not exhibit any observable toxicity in animals for all of the doses tested. In contrast, the R_2–R_6AANCK peptides induced immediate animal death at the highest dose (0.4 mmol/kg), with the overall animal survival depending on both the dose and arginine residue length (Table 2). Symptoms included instant jumping, hind-limb kicking, bulging eyes, and abnormal respiration. The animals that died did so within 1 min after peptide injection. Other studies on TAT (YGRKKRRQRRR), CTP (YGRRARRRRRR), and R_{11} peptides have demonstrated a similar high toxicity, with instant lethal effects observed at doses above 0.012, 0.010, and 0.012 mmol/kg, respectively.[57] A comparison of arginine-rich versus nonarginine peptides, such as TD (ACSSSPSKHCG) and GABA, revealed that mice survived only when exposed to the nonarginine peptides.[57,58] The employment of a higher dose of R_nAANCK peptide in this study was necessitated by our overall goal to

develop biocompatible theranostic agents for CEST MRI.[13] To achieve sufficient CEST MRI contrast enhancement beyond the endogenous background signal, the peptide concentration must exceed typical therapeutic levels. Taken together, these findings clearly demonstrate that CPP-associated toxicity is correlated with the number of arginine residues.

3.6. Hemocompatibility Studies.

One of the major challenges faced by the use of CPPs as a drug delivery system is their potential toxicity of membrane permeabilization, which may lyse red blood cells (RBC). Hence, in order to further investigate the potential mechanisms underlying the observed instant morbidity following i.v. injection of the higher R_n peptides at higher doses, the hemocompatibility of the R_1–R_6AANCK peptides and their effect on RBCs were studied using an *in vitro* hemolysis assay (Figure 5). We chose to test incubation concentrations of 3–100 mM *in vitro* in order to mimic the same blood concentrations *in vivo* after i.v. injection of 0.01–0.4 mmol/kg peptides. To convert this administration dose to the incubation concentration, we assumed an animal weight of 25 g. As an example, for a peptide containing two arginine units (molecular weight = 948) given at a dose of 0.01 mmol/kg, the amount of peptide injected in 100 μL is 0.296 mg. With an incubation volume of 100 μL for the hemolysis assay, the resulting concentration is 3 mM. This method was extended to determine the molar concentration for other doses for each peptide sequence. Significant hemolysis occurred for the higher R_n peptides at the higher doses, increasing with both the number of arginine residues and peptide concentration. R_1 did not show hemolytic effects for any concentration, corresponding to mice surviving all of the doses tested. R_2 exhibited 7% hemolysis at 100 mM, which was not statistically significant, but this dose was found to be lethal *in vivo*. Similarly, for R_3, insignificant hemolysis (9%) was observed for 50 mM, but this dose was also lethal. The results for the other R_4–R_6 peptides also showed that even a small amount of hemolysis can be fatal.

Arginine-rich peptides have been shown to be highly positively charged and can interact with the negatively charged phospholipids in the RBC membrane.[59,60] RBCs have a unique structure compared with other cells in the body, possessing a cell membrane that is thinner and more flexible. The RBC membrane also lacks certain proteins that are present in other cells, such as voltage-gated ion channels that regulate ion flow in excitable cells like neurons.[61] Furthermore, RBCs are exposed to high shear stress in the circulatory system, which makes their membrane more prone to mechanical stress and deformation.[62] This mechanical stress can lead to the formation of pores or defects in the membrane, which can make it more vulnerable to damage by arginine-rich peptides.[63] Despite the hemolysis being statistically insignificant for R_2 and R_3, the systemic effects provoked by even a small amount of RBC lysis were sufficient to cause near-instant mortality as a result of a cascade of deleterious systemic responses.[64] These include oxidative damage initiated by the release of hemoglobin into the bloodstream and depletion of nitric oxide by binding to hemoglobin, leading to instant vasoconstriction, resulting in a high mortality.[65]

3.7. *In Vivo* Biocompatibility Studies: Bone Marrow Function.

The biocompatibility of the R_1–R_6-AANCK peptides was investigated for bone marrow, liver, and kidney function. One week after i.v. injection, whole blood was collected and

analyzed for total blood cell counts (Figure 6). No significant difference in reticulocytes or RBCs could be observed. However, WBC counts showed a significant increase in $R_{4–6}$ at higher concentrations. Furthermore, the higher concentrations of R_4 and R_5 also caused a significant decrease in the platelet counts. The differences in WBCs suggest a potential immune response to the injected higher arginine component and not the AANCK itself (since this was kept constant). As for platelets, the vital cells in hemostasis, both the innate and adaptive immunity could have been affected. Activated platelets have thrombo-inflammatory functions that can link hemostasis and immune responses under various pathological conditions.[66] The high positive charge of the $R_{4–5}$ peptides may have contributed to this response, as it can lead to recognition by immune cells and activation of inflammatory pathways.[67] Moreover, the cell-penetrating properties could also be contributing factors, affecting the immune cells in the bloodstream or tissues.

3.8. *In Vivo* Biocompatibility Studies: Liver Function.

One week after i.v. injection of R_1–R_6-AANCK peptides, blood plasma was collected and analyzed for liver enzymes including aspartate transaminase (AST), alanine transaminase (ALT), and alkaline phosphatase (ALP) (Figure 7), with the elevated levels of these enzymes indicating liver damage. For R_1, R_2, R_3, and R_6, no significant differences in enzyme levels could be observed. However, a significant increase in the AST levels was observed at the highest concentrations of R_4 and R_5. Additionally, the highest concentration of R_5 also increased the ALP and ALT levels. However, histopathological analysis did not reveal any liver tissue damage for all peptide concentrations (Figure S2), suggesting that the elevation of these enzymes may be a transient effect rather than a result of sustained hepatic injury. One possibility is that the positive charge on R_5 facilitates its uptake into liver cells, where it disrupts normal cellular function and triggers an increase in enzyme production. Another possibility is that R_4 and R_5 interact with specific enzymes or regulatory proteins in the liver, leading to an increase in enzyme production. This hypothesis is supported by the fact that many enzymes involved in liver function are regulated by complex signaling pathways and that peptides and other small molecules can modulate these pathways in various ways.[68] Several studies have reported that cationic peptides, such as antimicrobial peptides, can induce liver damage by disrupting the liver cell membrane and causing cell death.[69] However, further studies are needed to determine the precise mechanism by which R_5 causes an increase in liver enzymes. For example, it would be important to investigate the intracellular localization of R_5 in liver cells as well as its effects on specific enzymes and signaling pathways. Such studies will be mandatory for potential clinical applications of arginine-rich peptides.

3.9. *In Vivo* Biocompatibility Studies: Kidney Function.

One week after i.v. injection of R_1–R_6-AANCK peptides, samples were collected for the analysis of creatinine, uric acid, blood urea nitrogen, albumin, and total protein (blood plasma), as well as creatinine and total protein (urine) (Figure 8). No significant changes outside the reference range for any of the assessed kidney factors were found. However, there was a trend in rising uric acid levels in blood plasma for the increasing concentrations of peptides and the number of arginine residues. An observable increase in creatinine and

total protein levels in urine was noted after administering 0.1 mmol/kg of R_3 and 0.5 mmol/kg of R_4, although they were still within the reference range.

Injection of 0.025 mmol/kg of R_5 resulted in an increase in creatinine and total protein levels in the urine as well, reaching the highest level of the reference range compared with the control mice. It is important to note that although all the observed changes in kidney function were within the reference range, possible indicators for early-stage kidney dysfunction may be present. Histopathological analysis of the kidney demonstrated no evidence of tissue damage or inflammation for all R_1–R_6 peptides (Figure S3). Previous studies have demonstrated that cationic polymers, such as polyarginine peptides, can accumulate in the kidney and cause nephrotoxicity by inducing oxidative stress and inflammation.[70] Therefore, the observed changes in kidney function parameters warrant further investigation into the potential nephrotoxic effects of R_1–R_6AANCK peptides, particularly at higher doses and later time points.

4. CONCLUSIONS

In summary, we demonstrated that higher numbers of arginine residues and peptide concentrations significantly boost their penetration into prostate cancer cells. However, our findings also caution against maximizing cell penetration. The observations of instant hemolysis and *in vivo* systemic toxicity, particularly impacting bone marrow, liver, and kidney functions, underscore a delicate balance between therapeutic efficacy and safety. As we move forward, these insights will be crucial for a safe development and clinical translation of drug/enzyme delivery systems.

Supplementary Material

Refer to Web version on PubMed Central for supplementary material.

ACKNOWLEDGMENTS

J.W.M.B. is supported by the National Institutes of Health (R01 EB030376 and P41 EB024495). I.B. is supported by the National Cancer Institute (R01 CA238025) and the National Institute of General Medical Sciences (1R35GM149272). M.T.M. is supported by the National Institutes of Health (P41 EB024495). The authors thank Dr. Yue Yuan (Anhui University of Science and Technology of China) for her valuable suggestions, comments, and inspiration for initiating legumain-based cell penetration studies.

REFERENCES

(1). Liu R; Chen Y; Liu G; Li C; Song Y; Cao Z; Li W; Hu J; Lu C; Liu Y PI3K/AKT Pathway as a Key Link Modulates the Multidrug Resistance of Cancers. Cell Death Dis. 2020, 11 (9), 797. [PubMed: 32973135]

(2). Zhang Q; Liu N; Wang J; Liu Y; Wang K; Zhang J; Pan X The Recent Advance of Cell-Penetrating and Tumor-Targeting Peptides as Drug Delivery Systems Based on Tumor Microenvironment. Mol. Pharmaceutics 2023, 20, 789 DOI: 10.1021/acs.molpharmaceut.2c00629.

(3). Khan MM; Filipczak N; Torchilin VP Cell penetrating peptides: A Versatile Vector for Co-delivery of Drug and Genes in Cancer. J. Controlled Release 2021, 330, 1220–1228.

(4). Strömstedt AA; Ringstad L; Schmidtchen A; Malmsten M Interaction Between Amphiphilic Peptides and Phospholipid Membranes. Curr. Opin. Colloid Interface Sci. 2010, 15 (6), 467–478.

(5). Nomura K; Kawano K; Kawaguchi Y; Kawamura Y; Michibata J; Kuwata K; Sugiyama K; Kusumoto K; Futaki S Hemopexin as a Potential Binding Partner of Arginine-Rich Cell-Penetrating Peptides in Serum. ACS Pharmacology & Translational Science 2022, 5 (8), 603–615. [PubMed: 35983275]

(6). Pan L; He Q; Liu J; Chen Y; Ma M; Zhang L; Shi J Nuclear-targeted Drug Delivery of TAT Peptide-Conjugated Monodisperse Mesoporous Silica Nanoparticles. J. Am. Chem. Soc. 2012, 134 (13), 5722–5725. [PubMed: 22420312]

(7). Mansur AA; Carvalho SM; Lobato ZI; Leite MDF; Cunha ADS Jr; Mansur HS Design and Development of Polysaccharide-Doxorubicin-Peptide Bioconjugates for Dual Synergistic Effects of Integrin-Targeted and Cell-Penetrating Peptides for Cancer Chemotherapy. Bioconjugate Chem. 2018, 29 (6), 1973–2000.

(8). Zhang L; Jiang C; Zeng F; Zhou H; Li D; He X; Shen S; Yang X; Wang J A Polymeric Nanocarrier with a Tumor Acidity-activatable Arginine-rich (R 9) Peptide for Enhanced Drug Delivery. Biomaterials science 2020, 8 (8), 2255–2263. [PubMed: 32129378]

(9). Yin J; Liu D; Bao L; Wang Q; Chen Y; Hou S; Yue Y; Yao W; Gao X Tumor Targeting and Microenvironment-Responsive Multifunctional Fusion Protein for Pro-Apoptotic Peptide Delivery. Cancer letters 2019, 452, 38–50. [PubMed: 30904618]

(10). Zhou M; Zou X; Cheng K; Zhong S; Su Y; Wu T; Tao Y; Cong L; Yan B; Jiang Y The Role of Cell-Penetrating Peptides in Potential Anti-Cancer Therapy. Clin. Transl. Med. 2022, 12 (5), No. e822. [PubMed: 35593206]

(11). Yuan Y; Bulte JWM Enzyme-Mediated Intratumoral Self-Assembly of Nanotheranostics for Enhanced Imaging and Tumor Therapy. WIREs Nanomed. Nanobiotechnol. 2022, 14 (4), No. e1786.

(12). Levin A; Hakala TA; Schnaider L; Bernardes GJ; Gazit E; Knowles TP Biomimetic Peptide Self-Assembly for Functional Materials. Nature Reviews Chemistry 2020, 4 (11), 615–634.

(13). Yuan Y; Zhang J; Qi X; Li S; Liu G; Siddhanta S; Barman I; Song X; McMahon MT; Bulte JW Furin-Mediated Intracellular Self-Assembly of Olsalazine Nanoparticles for Enhanced Magnetic Resonance Imaging and Tumour Therapy. Nature materials 2019, 18 (12), 1376–1383. [PubMed: 31636420]

(14). Yuan Y; Raj P; Zhang J; Siddhanta S; Barman I; Bulte JWM Furin-Mediated Self-Assembly of Olsalazine Nanoparticles for Targeted Raman Imaging of Tumors. Angew. Chem., Int. Ed. 2021, 60 (8), 3923–3927.

(15). Tanwar S; Ghaemi B; Raj P; Singh A; Wu L; Yuan Y; Arifin DR; McMahon MT; Bulte JWM; Barman I A Smart Intracellular Self-Assembling Bioorthogonal Raman Active Nanoprobe for Targeted Tumor Imaging. Adv. Sci. (Weinh) 2023, 10, No. e2304164. [PubMed: 37715297]

(16). Tanwar S; Wu L; Zahn N; Raj P; Ghaemi B; Chatterjee A; Bulte JWM; Barman I Targeted Enzyme Activity Imaging with Quantitative Phase Microscopy. Nano Lett. 2023, 23 (10), 4602–4608. [PubMed: 37154678]

(17). Lafarga V; Sirozh O; Díaz-López I; Galarreta A; Hisaoka M; Zarzuela E; Boskovic J; Jovanovic B; Fernandez-Leiro R; Munñoz J Widespread Displacement of DNA-and RNA-Binding Factors Underlies Toxicity of Arginine-Rich Cell-Penetrating Peptides. EMBO J. 2021, 40 (13), No. e103311. [PubMed: 33978236]

(18). Chen C; Yamanaka Y; Ueda K; Li P; Miyagi T; Harada Y; Tezuka S; Narumi S; Sugimoto M; Kuroda M Phase Separation and Toxicity of C9orf72 poly (PR) Depends on Alternate Distribution of Arginine. J. Cell Biol. 2021, 220 (11), No. e202103160. [PubMed: 34499080]

(19). Moens TG; Niccoli T; Wilson KM; Atilano ML; Birsa N; Gittings LM; Holbling BV; Dyson MC; Thoeng A; Neeves J C9orf72 Arginine-Rich Dipeptide Proteins Interact with Ribosomal Proteins In Vivo to Induce a Toxic Translational Arrest that is Rescued by eIF1A. Acta Neuropathol. 2019, 137, 487–500. [PubMed: 30604225]

(20). Cerulli RA; Shehaj L; Tosic I; Jiang K; Wang J; Frank DA; Kritzer JA Cytosolic Delivery of Peptidic STAT3 SH2 Domain Inhibitors. Bioorganic & medicinal chemistry 2020, 28 (12), No. 115542. [PubMed: 32503696]

(21). Mura S; Nicolas J; Couvreur P Stimuli-Responsive Nanocarriers for Drug Delivery. Nat. Mater. 2013, 12 (11), 991–1003. [PubMed: 24150417]

(22). Yang Y; Hong H; Zhang Y; Cai W Molecular Imaging of Proteases in Cancer. Cancer Growth Metastasis 2009, 2, 13–27. [PubMed: 20234801]

(23). Liu C; Sun C; Huang H; Janda K; Edgington T Overexpression of Legumain in Tumors is Significant for Invasion/Metastasis and a Candidate Enzymatic Target for Prodrug Therapy. Cancer Res. 2003, 63 (11), 2957–2964. [PubMed: 12782603]

(24). Ohno Y; Nakashima J; Izumi M; Ohori M; Hashimoto T; Tachibana M Association of Legumain Expression Pattern with Prostate Cancer Invasiveness and Aggressiveness. World J. Urol 2013, 31 (2), 359–364. [PubMed: 23124822]

(25). Poreba M Recent Advances in the Development of Legumain-Selective Chemical Probes and Peptide Prodrugs. Biol. Chem. 2019, 400 (12), 1529–1550. [PubMed: 31021817]

(26). Clees AS; Stolp V; Häupl B; Fuhrmann DC; Wempe F; Seibert M; Weber S; Banning A; Tikkanen R; Williams R; Bruüne B Identification of the Cysteine Protease Legumain as a Potential Chronic Hypoxia-Specific Multiple Myeloma Target Gene. Cells 2022, 11 (2), 292. [PubMed: 35053409]

(27). Zhao Y; Hai Z; Wang H; Su L; Liang G Legumain-Specific Near-Infrared Fluorescence ″Turn On″ for Tumor-Targeted Imaging. Anal. Chem. 2018, 90 (15), 8732–8735. [PubMed: 30027744]

(28). Wang Q; Lu C; Li K; Xia Y; Qiu L; Lin J Legumain-Mediated Self-Assembly of a (131)I-labelled Agent for Targeted Radiotherapy of Tumors. J. Mater. Chem. B 2022, 10 (13), 2251–2259. [PubMed: 35297450]

(29). Liu J; Afshar S In vitro Assays: Friends or Foes of Cell-Penetrating Peptides. International Journal of Molecular Sciences 2020, 21 (13), 4719. [PubMed: 32630650]

(30). Nakase I; Takeuchi T; Tanaka G; Futaki S Methodological and Cellular Aspects that Govern the Internalization Mechanisms of Arginine-Rich Cell-Penetrating Peptides. Advanced drug delivery reviews 2008, 60 (4–5), 598–607. [PubMed: 18045727]

(31). Traboulsi H; Larkin H; Bonin M-A; Volkov L; Lavoie CL; Marsault E Macrocyclic cell penetrating peptides: A Study of Structure-Penetration Properties. Bioconjugate Chem. 2015, 26 (3), 405–411.

(32). Dougherty PG; Sahni A; Pei D Understanding Cell Penetration of Cyclic Peptides. Chem. Rev. 2019, 119 (17), 10241–10287. [PubMed: 31083977]

(33). Gautam A; Sharma M; Vir P; Chaudhary K; Kapoor P; Kumar R; Nath SK; Raghava GP Identification and Characterization of Novel Protein-Derived Arginine-Rich Cell-Penetrating Peptides. Eur. J. Pharm. Biopharm. 2015, 89, 93–106. [PubMed: 25459448]

(34). Nakase I; Noguchi K; Aoki A; Takatani-Nakase T; Fujii I; Futaki S Arginine-Rich Cell-Penetrating Peptide-Modified Extracellular Vesicles for Active Macropinocytosis Induction and Efficient Intracellular Delivery. Sci. Rep. 2017, 7 (1), 1991. [PubMed: 28512335]

(35). Åmand HL; Rydberg HA; Fornander LH; Lincoln P; Nordén B; Esbjörner EK Cell Surface Binding and Uptake of Arginine-and Lysine-Rich Penetratin Peptides in Absence and Presence of Proteoglycans. Biochimica et biophysica acta (BBA)-biomembranes 2012, 1818 (11), 2669–2678. [PubMed: 22705501]

(36). Reissmann S Cell Penetration: Scope and Limitations by the Application of Cell-Penetrating Peptides. Journal of Peptide Science 2014, 20 (10), 760–784. [PubMed: 25112216]

(37). Mello LR; Aguiar RB; Yamada RY; Moraes JZ; Hamley IW; Alves WA; Reza M; Ruokolainen J; Silva ER Amphipathic Design Dictates Self-assembly, Cytotoxicity and Cell Uptake of Arginine-Rich Surfactant-Like Peptides. J. Mater. Chem. B 2020, 8 (12), 2495–2507. [PubMed: 32108843]

(38). Naik RJ; Chatterjee A; Ganguli M Different Roles of Cell Surface and Exogenous Glycosaminoglycans in Controlling Gene Delivery by Arginine-Rich Peptides with Varied Distribution of Arginines. Biochimica et Biophysica Acta (BBA)-Biomembranes 2013, 1828 (6), 1484–1493. [PubMed: 23454086]

(39). Takechi-Haraya Y; Aki K; Tohyama Y; Harano Y; Kawakami T; Saito H; Okamura E Glycosaminoglycan Binding and Non-Endocytic Membrane Translocation of Cell-Permeable Octaarginine Monitored by Real-Time in-cell NMR Spectroscopy. Pharmaceuticals 2017, 10 (2), 42. [PubMed: 28420127]

(40). Ziegler A; Seelig J Contributions of Glycosaminoglycan Binding and Clustering to the Biological Uptake of the Non-amphipathic Cell-Penetrating Peptide WR9. Biochemistry 2011, 50 (21), 4650–4664. [PubMed: 21491915]

(41). Ziegler A; Seelig J Interaction of the Protein Transduction Domain of HIV-1 TAT with Heparan Sulfate: Binding Mechanism and Thermodynamic Parameters. Biophysical journal 2004, 86 (1), 254–263. [PubMed: 14695267]

(42). Reid LM; Verma CS; Essex JW The Role of Molecular Simulations in Understanding the Mechanisms of Cell-Penetrating Peptides. Drug Discovery Today 2019, 24 (9), 1821–1835. [PubMed: 31229665]

(43). Tietz O; Cortezon-Tamarit F; Chalk R; Able S; Vallis KA Tricyclic Cell-Penetrating Peptides for Efficient Delivery of Functional Antibodies Into Cancer Cells. Nat. Chem. 2022, 14 (3), 284–293. [PubMed: 35145246]

(44). Herce HD; Garcia AE Molecular Dynamics Simulations Suggest a Mechanism for Translocation of the HIV-1 TAT Peptide Across Lipid Membranes. Proc. Natl. Acad. Sci. U. S. A. 2007, 104 (52), 20805–20810. [PubMed: 18093956]

(45). Brock R The Uptake of Arginine-Rich Cell-Penetrating Peptides: Putting the Puzzle Together. Bioconjugate Chem. 2014, 25 (5), 863–868.

(46). Rothbard JB; Kreider E; VanDeusen CL; Wright L; Wylie BL; Wender PA Arginine-Rich Molecular Transporters for Drug Delivery: Role of Backbone Spacing in Cellular Uptake. Journal of medicinal chemistry 2002, 45 (17), 3612–3618. [PubMed: 12166934]

(47). Ohno Y; Nakashima J; Izumi M; Ohori M; Hashimoto T; Tachibana M Association of Legumain Expression Pattern with Prostate Cancer Invasiveness and Aggressiveness. World journal of urology 2013, 31, 359–364. [PubMed: 23124822]

(48). Mi X; Guo X; Du H; Han M; Liu H; Luo Y; Wang D; Xiang R; Yue S; Zhang Y Combined Legumain-and Integrin-Targeted Nanobubbles for Molecular Ultrasound Imaging of Breast Cancer. Nanomedicine 2022, 42, No. 102533. [PubMed: 35150904]

(49). Spiciarich DR; Nolley R; Maund SL; Purcell SC; Herschel J; Iavarone AT; Peehl DM; Bertozzi CR Bioorthogonal Labeling of Human Prostate Cancer Tissue Slice Cultures for Glycoproteomics. Angew. Chem., Int. Ed. 2017, 56 (31), 8992–8997.

(50). Reddy BD; Beeraka NM; Chitturi C; Madhunapantula SV An Overview of Targeting Legumain for Inhibiting Cancers. Curr. Pharm. Des. 2021, 27 (31), 3337–3348. [PubMed: 33238867]

(51). Ruan S; Xie R; Qin L; Yu M; Xiao W; Hu C; Yu W; Qian Z; Ouyang L; He Q Aggregable Nanoparticles-Enabled Chemotherapy and Autophagy Inhibition Combined with Anti-PD-L1 Antibody for Improved Glioma Treatment. Nano Lett. 2019, 19 (11), 8318–8332. [PubMed: 31610656]

(52). Ness KA; Eddie SL; Higgins CA; Templeman A; D'Costa Z; Gaddale KK; Bouzzaoui S; Jordan L; Janssen D; Harrison T Development of a Potent and Selective Cell Penetrant Legumain Inhibitor. Bioorg. Med. Chem. Lett. 2015, 25 (23), 5642–5645. [PubMed: 26522952]

(53). Liang G; Ronald J; Chen Y; Ye D; Pandit P; Ma ML; Rutt B; Rao J Controlled Self-Assembling of Gadolinium Nanoparticles as "Smart" Molecular Magnetic Resonance Imaging Contrast Agents. Angewandte Chemie (International ed. in English) 2011, 50 (28), 6283. [PubMed: 21618367]

(54). Yuan Y; Wang F; Tang W; Ding Z; Wang L; Liang L; Zheng Z; Zhang H; Liang G Intracellular Self-Assembly of Cyclic d-Luciferin Nanoparticles for Persistent Bioluminescence Imaging of Fatty Acid Amide Hydrolase. ACS Nano 2016, 10 (7), 7147–7153. [PubMed: 27348334]

(55). Liang G; Ren H; Rao J A Biocompatible Condensation Reaction for Controlled Assembly of Nanostructures in Living Cells. Nature Chem. 2010, 2 (1), 54–60. [PubMed: 21124381]

(56). Tanwar S; Ghaemi B; Raj P; Singh A; Wu L; Yuan Y; Arifin DR; McMahon MT; Bulte JW; Barman I A Smart Intracellular Self-Assembling Bioorthogonal Raman Active Nanoprobe for Targeted Tumor Imaging. Adv. Sci. 2023, 10, No. 2304164.

(57). Li Q; Xu M; Cui Y; Huang C; Sun M Arginine-Rich Membrane-Permeable Peptides are Seriously Toxic. Pharmacol. Res. Perspect. 2017, 5 (5), No. e00334. [PubMed: 28971613]

(58). Grogg M; Hilvert D; Ebert MO; Beck AK; Seebach D; Kurth F; Dittrich PS; Sparr C; Wittlin S; Rottmann M Cell Penetration, Herbicidal Activity, and In-Vivo-Toxicity of Oligo-

Arginine Derivatives and of Novel Guanidinium-Rich Compounds Derived from the Biopolymer Cyanophycin. Helv. Chim. Acta 2018, 101 (10), No. e1800112. [PubMed: 30905972]

(59). Edwards AB; Mastaglia FL; Knuckey NW; Yip K-H; Meloni B Assessment of the Safety of the Cationic Arginine-Rich Peptides (CARPs) Poly-Arginine-18 (R18 and R18D) in Ex Vivo Models of Mast Cell Degranulation and Red Blood Cell Hemolysis. Biochemistry and Biophysics Reports 2022, 31, No. 101305. [PubMed: 35812346]

(60). Hong J; Oren Z; Shai Y Structure and Organization of Hemolytic and Nonhemolytic Diastereomers of Antimicrobial Peptides in Membranes. Biochemistry 1999, 38 (51), 16963–16973. [PubMed: 10606532]

(61). Pagano M; Faggio C The Use of Erythrocyte Fragility to Assess Xenobiotic Cytotoxicity. Cell biochemistry and function 2015, 33 (6), 351–355. [PubMed: 26399850]

(62). De Oliveira S; Saldanha C An Overview About Erythrocyte Membrane. Clinical hemorheology and microcirculation 2010, 44 (1), 63–74. [PubMed: 20134094]

(63). Herce H; Garcia A; Litt J; Kane R; Martín P; Enrique N; Rebolledo A; Milesi V Arginine-Rich Peptides Destabilize the Plasma Membrane, Consistent with a Pore Formation Translocation Mechanism of Cell-Penetrating Peptides. Biophysical journal 2009, 97 (7), 1917–1925. [PubMed: 19804722]

(64). Roumenina LT; Bartolucci P; Pirenne F The Role of Complement in Post-Transfusion Hemolysis and Hyperhemolysis Reaction. Transfusion medicine reviews 2019, 33 (4), 225–230. [PubMed: 31672341]

(65). Hod E Consequences of Hemolysis: Pro-Inflammatory Cytokine Response to Erythrophagocytosis. Transfusion Clinique et Biologique 2019, 26 (2), 125–127. [PubMed: 30862396]

(66). Dib PRB; Quirino-Teixeira AC; Merij LB; Pinheiro MBM; Rozini SV; Andrade FB; Hottz ED Innate Immune Receptors in Platelets and Platelet-Leukocyte Interactions. Journal of Leucocyte Biology 2020, 108 (4), 1157–1182.

(67). Lopez-Silva TL; Leach DG; Azares A; Li I-C; Woodside DG; Hartgerink JD Chemical Functionality of Multidomain Peptide Hydrogels Governs Early Host Immune Response. Biomaterials 2020, 231, No. 119667. [PubMed: 31855625]

(68). Rudling M; Angelin B; Ståhle L; Reihnér E; Sahlin S; Olivecrona H; Björkhem I; Einarsson C Regulation of Hepatic Low-Density Lipoprotein Receptor, 3-hydroxy-3-Methylglutaryl Coenzyme A Reductase, and Cholesterol 7α-hydroxylase mRNAs in Human Liver. Journal of Clinical Endocrinology & Metabolism 2002, 87 (9), 4307–4313. [PubMed: 12213890]

(69). Aguilera TA; Olson ES; Timmers MM; Jiang T; Tsien RY Systemic In Vivo Distribution of Activatable Cell Penetrating Peptides is Superior to that of Cell Penetrating Peptides. Integrative Biology 2009, 1 (5–6), 371–381. [PubMed: 20023744]

(70). Samal SK; Dash M; Van Vlierberghe S; Kaplan DL; Chiellini E; Van Blitterswijk C; Moroni L; Dubruel P Cationic Polymers and Their Therapeutic Potential. Chem. Soc. Rev. 2012, 41 (21), 7147–7194. [PubMed: 22885409]

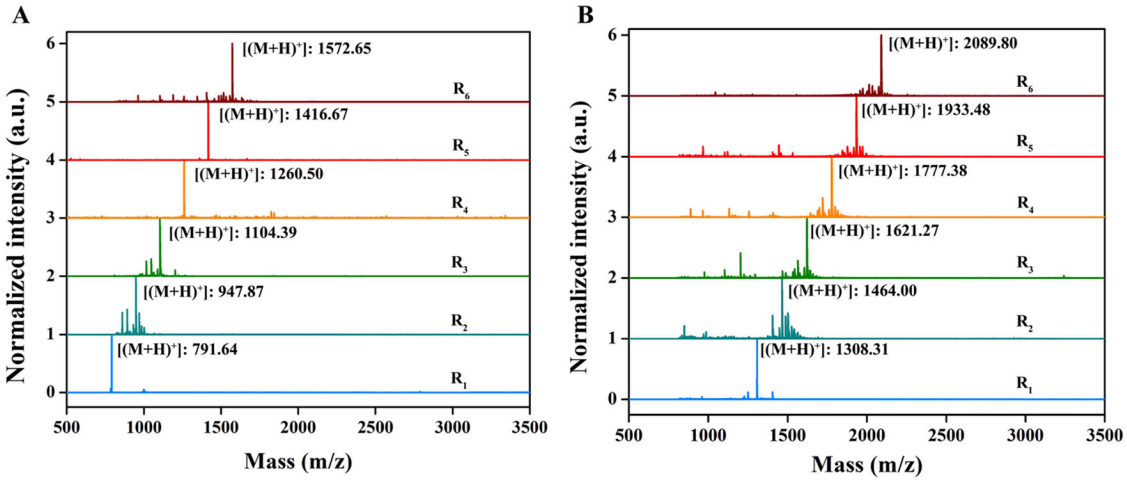

Figure 1.

(A) MALDI-TOF characterization of unlabeled R_1–R_6AANCK and (B) Alexa Fluor 488-conjugated R_1–R_6AANCK peptides.

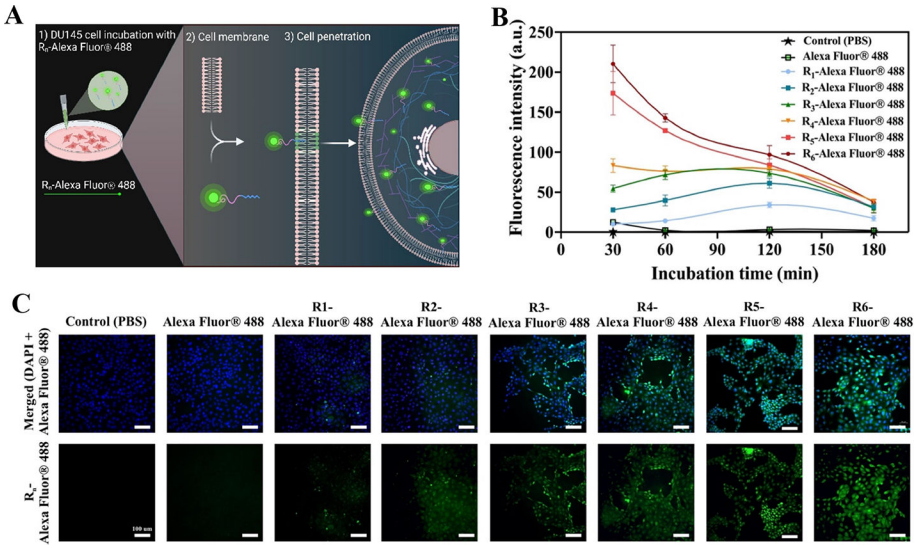

Figure 2.

(A) Schematic outline of experiments on the cellular penetration of Alexa Fluor 488-conjugated peptides. (B) Time-dependent DU145 prostate cancer cell penetration of R_1–R_6-AANCK-Alexa Fluor 488 after 30, 60, 90, 120, and 180 min of incubation with 50 μM Alexa Fluor 488-conjugated peptides. (C) Confocal microscopy of DU145 cells 60 min after incubation with 50 μM R_1–R_6-AANCK-Alexa Fluor 488-conjugated peptides. Scale bar: 100 μm.

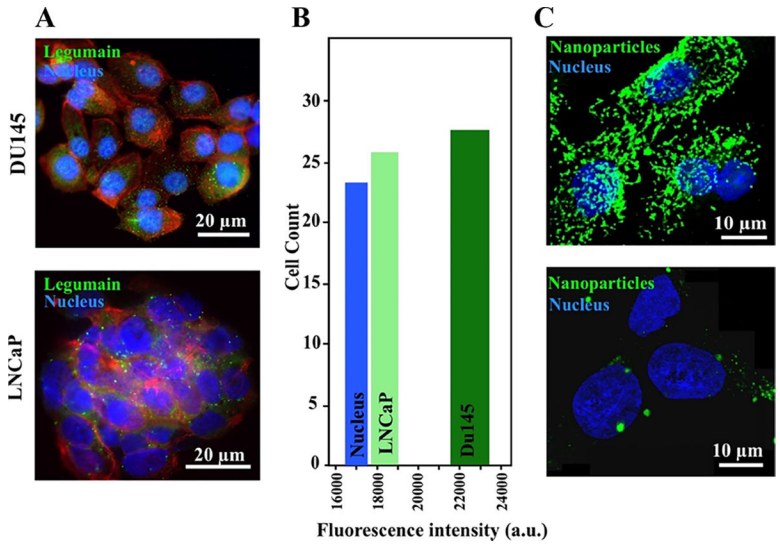

Figure 3.

(A) Fluorescence microscopy and (B) quantification of legumain expression in DU145 and LNCaP prostate tumor cells (C). Fluorescence microscopy shows extensive intracellular self-assembly of fluorescent NPs after the incubation of Alexa-R_6AAN-CBT peptide with DU145 cells but not LNCaP cells. Legumain is depicted in green, phalloidin is in red, and the nucleus is stained blue.

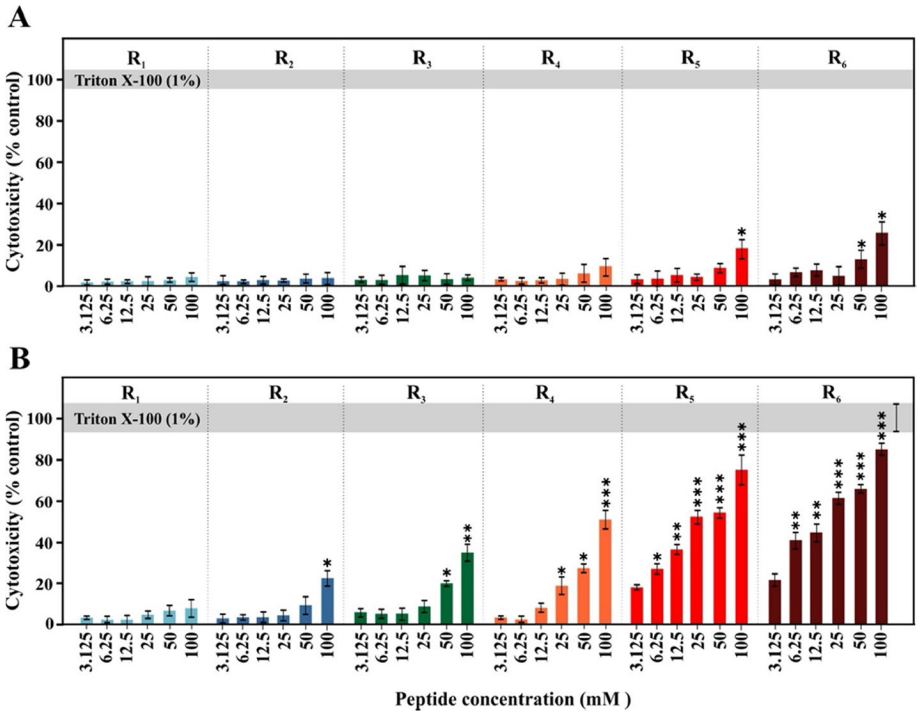

Figure 4.

In vitro cytotoxicity assessment of R_1–R_6AANCK peptides for DU145 cells after (A) 2 h and (B) 48 h incubation with 3.125, 6.25, 12.5, 25, 50, or 100 mM peptide. *P*-values <0.001 (***), < 0.01 (**), and <0.05 (*) were considered significant (n = 6 repeats). Triton-X treatment was used as positive (100% cytotoxicity) control.

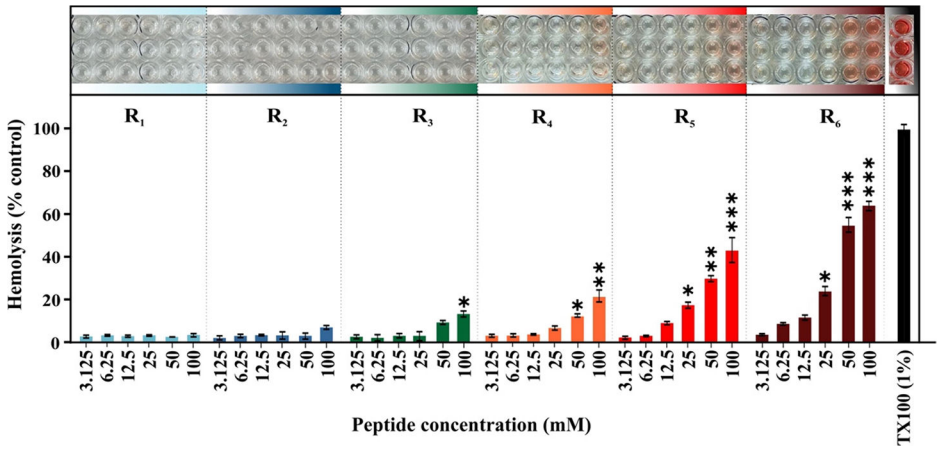

Figure 5.

Hemolytic activity of R_1–R_6 AANCK peptides at different concentrations (mM). 1% Triton X-100 was included as a positive control. *P*-values <0.001 (***), < 0.01 (**), and <0.05 (*) were considered significant (n = 6 repeats).

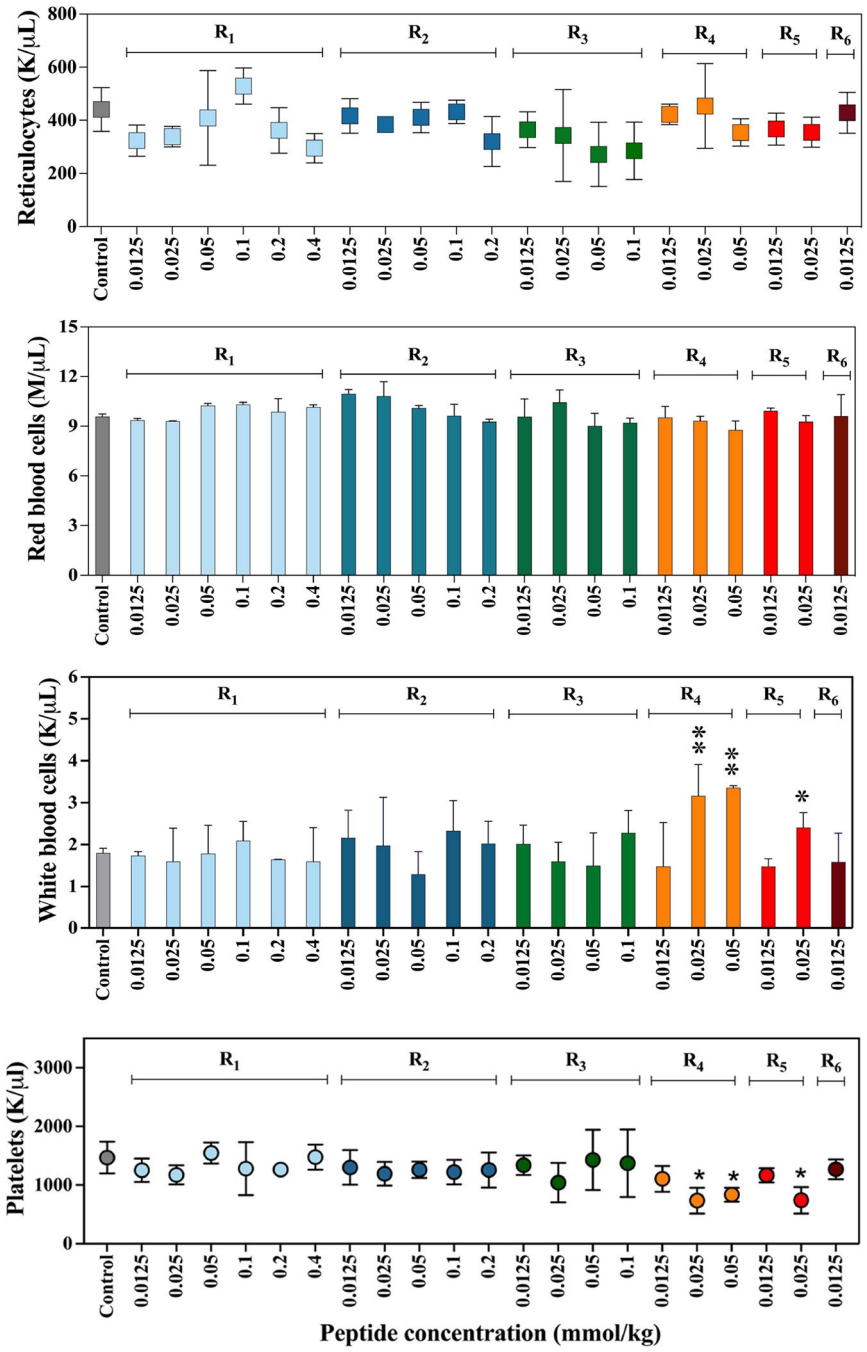

Figure 6.

Biocompatibility of R_1–R_6AANCK peptides on the bone marrow function. *P*-values <0.001 (***), < 0.01 (**), and <0.05 (*) were considered significant ($n = 3$ each).

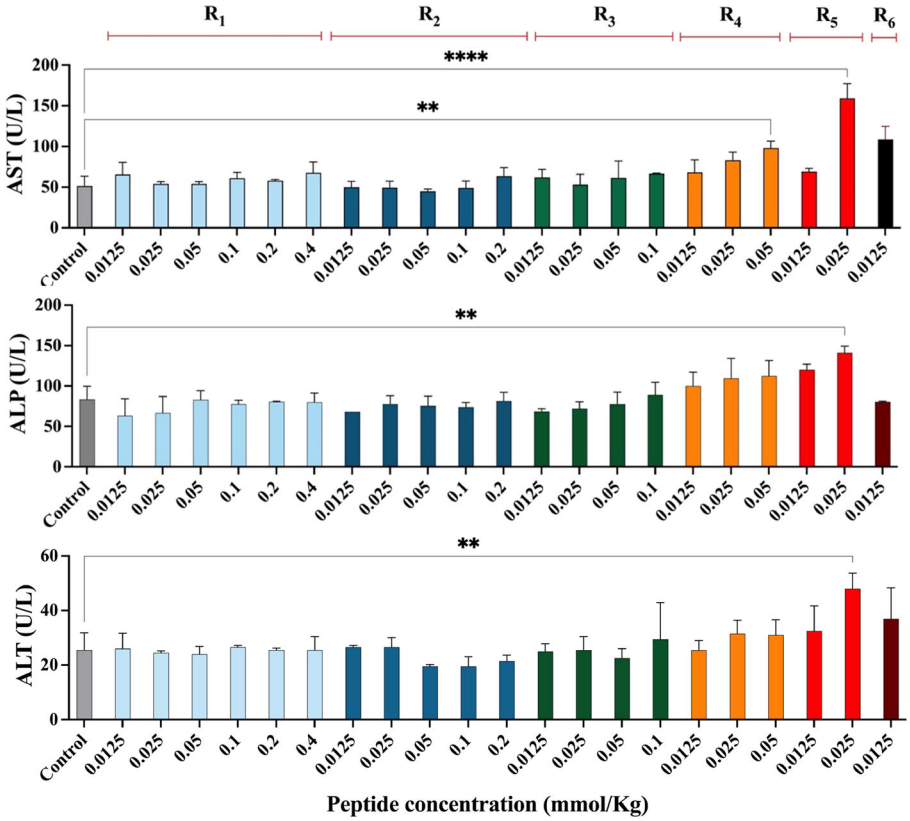

Figure 7.

Biocompatibility of R_1–R_6AANCK peptides on liver function. *P*-values <0.0001 (****), < 0.001 (***), < 0.01 (**), and <0.05 (*) were considered significant (n = 3 each).

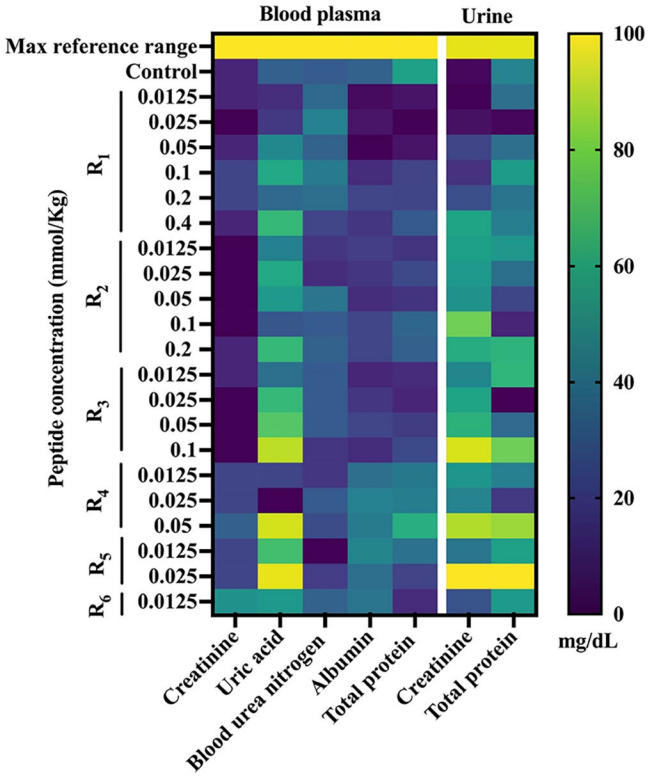

Figure 8.

Biocompatibility of R_1–R_6AANCK peptides on kidney function. *P*-values <0.0001 (****), < 0.001 (***), < 0.01 (**), and <0.05 (*) were considered significant ($n = 3$ each).

Table 1.

R_1-R_6-AANCK Peptide Composition and Characterization

Peptide sequence	Chemical structure	Molecular weight (Dalton)	Arginine content (%)	Overall charge	CP50 (60 min)	CP50 (120 min)
RAANCK (R_1)	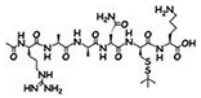	791.99	16.6	+2	75±12 μM	32±5 μM
RRAANCK (R_2)	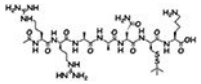	948.17	28.5	+3	30±5 μM	12±2 μM
RRRAANCK (R_3)	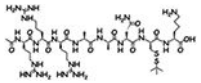	1104.36	37.5	+4	8.5±2.0 μM	8.9±2.1 μM
RRRRAANCK (R_4)	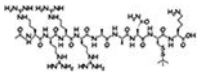	1260.55	44.4	+5	3.2±1 μM	7.8±1.4 μM
RRRRRAANCK (R_5)	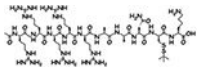	1416.74	50	+6	1.3±0.5 μM	5.2±1.2 μM
RRRRRRAANCK (R_6)	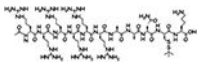	1572.93	54.5	+7	0.8±0.3 μM	2.1±0.6 μM

ACS Appl Mater Interfaces. Author manuscript; available in PMC 2024 August 30.

Table 2.

Animal Survival (n = 3 Each)[a]

	peptide (R_nAANCK)					
dose (mmol/kg)	**R_1**	**R_2**	**R_3**	**R_4**	**R_5**	**R_6**
0.4	+	−	−	−	−	−
0.2	+	+	−	−	−	−
0.1	+	+	+	−	−	−
0.05	+	+	+	+	−	−
0.025	+	+	+	+	+	−
0.0125	+	+	+	+	+	+

[a] + = survival, − = no survival.